

Hyperspectral Imaging for Intelligence, Surveillance, and Reconnaissance

David Stein, Jon Schoonmaker, and Eric Coolbaugh
SSC San Diego

INTRODUCTION

The optical spectrum is generally considered to include the ultraviolet (200 to 400 nm), the visible (400 to 700 nm), the near infrared (700 to 1100 nm), and the short-wave infrared (1100 to 2500 nm). Sensors operating in these bands detect reflected light which is used to discriminate an object from its background and to classify it based on spectral characteristics. Spectral sensors capitalize on the color difference between objects and the background. A color video camera that divides the reflected light into red, green, and blue components is thus a simple spectral sensor. More complicated sensors break the spectrum into finer and finer bands and/or selectively tune to bands appropriate for a specific object or background. In general, a multispectral sensor, illustrated in Figure 1, is defined as a sensor using two to tens of bands, while a hyperspectral sensor, illustrated in Figure 2, is defined as a sensor using tens to hundreds of bands. Spectral sensors are divided into four types or approaches. Currently, the most common type is the "pushbroom" hyperspectral sensor. In this approach (Figure 2), a single line is imaged through a dispersing element so that the line is imaged in many different bands (colors) simultaneously. A second spatial dimension is realized through sensor motion. A second type is a multispectral filter wheel system in which a scene is imaged consecutively in multiple bands. A third type images multiple bands simultaneously using multiple chips (or multiple areas on the same chip). This approach uses multiple apertures or a splitting technique, such as a series of dichroic prisms or a tetrahedral mirror or lens. The fourth approach is the use of a Fourier transform spectrometer. The product of any of these sensors is an image cube as illustrated in Figure 3.

Hyperspectral Imaging at SSC San Diego

SSC San Diego has supported a number of hyperspectral programs over the last several years for a variety of government agencies, including the Defense Advanced Research Projects Agency (DARPA), the Spectral Information and Technology Assessment Center (SITAC), the Office of Naval Research (ONR), the Office of the Secretary of Defense (OSD), and the High Performance Computing Management Office (HPCMO). We have worked on DARPA's Adaptive Spectral Reconnaissance Program (ASRP), the goal of which was to demonstrate the detection of concealed terrestrial military targets and the cueing of a high-resolution imager. For ONR, we have been involved with maritime applications of

ABSTRACT

This paper highlights SSC San Diego contributions to the research and development of hyperspectral technology. SSC San Diego developed the real-time, onboard hyperspectral data processor for automated cueing of high-resolution imagery as part of the Adaptive Spectral Reconnaissance Program (ASRP), which demonstrated a practical solution to broad area search by leveraging hyperspectral phenomenology. SSC San Diego is now implementing the ASRP algorithm suite on parallel processors, using a portable, scalable architecture that will be remotely accessible. SSC San Diego performed the initial demonstrations that led to the Littoral Airborne Sensor Hyperspectral (LASH) program, which applies hyperspectral imaging to the problem of submarine detection in the littoral zone. Under the In-house Laboratory Independent Research (ILIR) program, SSC San Diego has developed new and enhanced methods for hyperspectral analysis and exploitation.

hyperspectral sensors. Under OSD sponsorship, we have demonstrated the capabilities of hyperspectral remote sensing for search and rescue applications. For SITAC, we have provided ground truth measurements of ocean optical properties and illumination required for controlled experiments, and we have analyzed the bands required for optimal ocean imaging. The HPCMO is sponsoring our work to develop scalable and portable implementations of the ASRP algorithms. Under ONR and SSC San Diego In-house Laboratory Independent Research (ILIR) funding, we have developed new and enhanced methods for hyperspectral analysis and exploitation. Highlights of these efforts are described in more detail below.

Terrestrial Hyperspectral Remote Sensing

The DARPA ASRP successfully demonstrated the capability to detect military targets of interest in real time by using an airborne hyperspectral system to cue high-resolution images for ground analysis. SSC San Diego led all research, development, coding, and implementation of the end-to-end processing and critical hyperspectral detection and recognition algorithms. The algorithms and processing architecture developed are applicable to a broad scope of missions, targets of interest, and platform architectures. ASRP pushed the state of the art beyond simple detection of targets in the open, making detection of difficult, realistically positioned targets possible at low false alarm rates. Figure 4 shows the difficult environment, used by ASRP for real-time hyperspectral system demonstrations, that may be encountered during military operations. The variety of natural and man-made materials and the

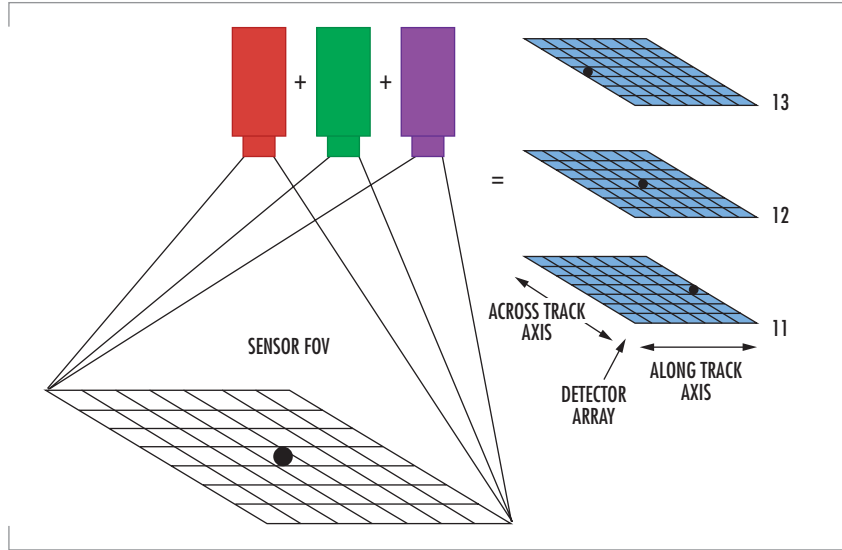


FIGURE 1. Schematic of three-band multispectral imaging camera.

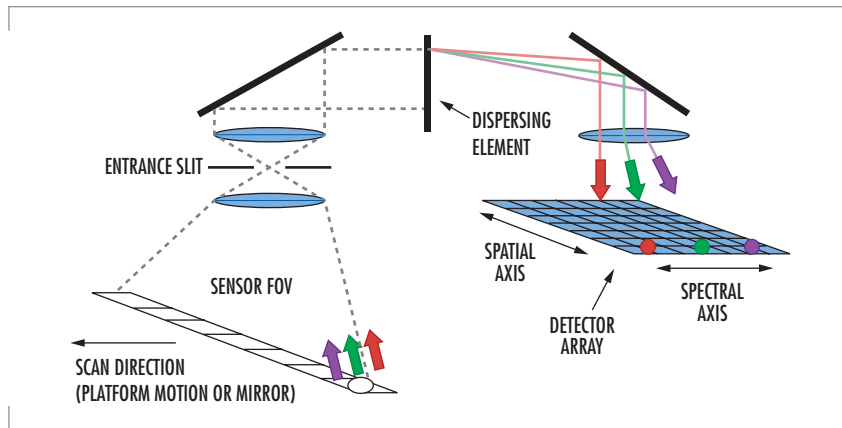


FIGURE 2. Schematic of a pushbroom dispersive hyperspectral sensor.

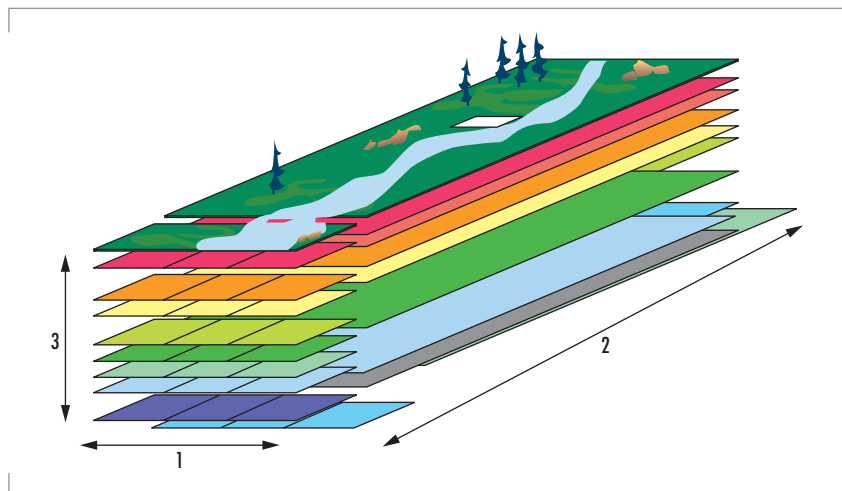


FIGURE 3. Hyperspectral image cube's cross-track, 1; along track, 2; and spectral dimension, 3.

variability of illumination combine to form a highly complex spectral detection challenge. Figure 5 compares the visibility of two targets in high-resolution imagery (top), in a red-green-blue (RGB) image (middle), and in the output of a detection statistic (bottom). These detections exemplify the ability of the hyperspectral system to identify target positions even when they may not be evident in traditional high-resolution imagery.

The High Performance Computing Management Office (HPCMO) has funded SSC San Diego, as part of the Hyperspectral Information Exploitation Project, to implement the ASRP hyperspectral algorithm suite and end-to-end processing on high-performance computer (HPC) platforms in a portable, scalable architecture accessible by a wide variety of Government users. Parallel processing capabilities will provide a new dimension for hyperspectral processing, allowing multiple hyperspectral algorithms to optimize target detection and recognition on massive data sets.

Maritime Sensor Systems

SSC San Diego has been instrumental in initiating and demonstrating the use of hyperspectral imagery for surveillance of the littoral. In 1996, SETS Technology, working with SSC San Diego, flew the SETS Technology Advanced Airborne Hyperspectral Imaging System (AAHIS) over submarines at the Pacific Missile Range Facility northwest of Kauai. The results of these flights led to the Littoral Airborne Sensor Hyperspectral (LASH) program.

LASH is an integrated optical sensor system that uses pushbroom scanning for the detection of submarines in the littoral environment. The LASH system consists of a



FIGURE 4. Three-color image of an ASRP hyperspectral image.

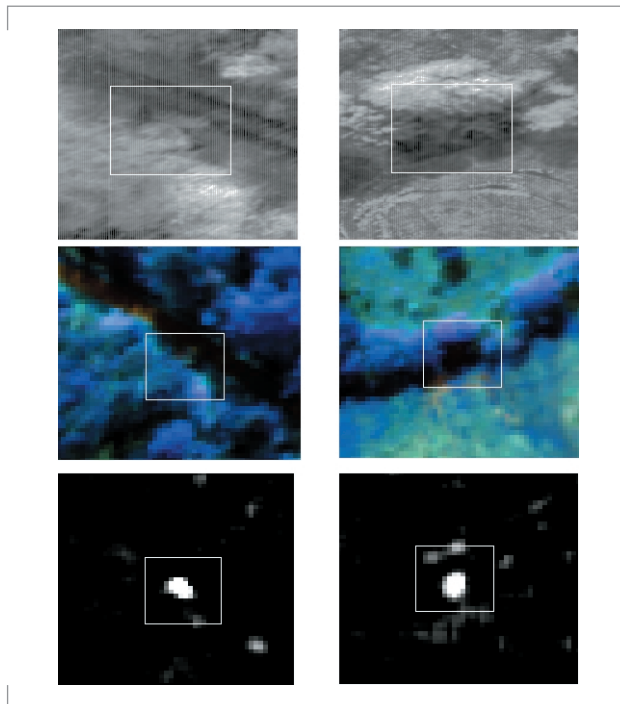


FIGURE 5. These figures show a high-resolution panchromatic imager (6-inch ground sample distance [GSD]) [top], and RGB image created from three hyperspectral bands (1-meter GSD) [middle], and one hyperspectral algorithm detection statistic image [bottom] for two different targets hidden along tree lines in shadow.

passive hyperspectral imager (HSI) assembly, an image processor, a data storage (archival) unit, a data display unit for operator use that incorporates the system monitoring, and control functions. The system is integrated into a modified ALE-43 (chaff cutter and dispenser pod) and mounted on a standard pylon at wing station 12 (Figure 6). All principal elements of the LASH system are contained within the pod. The units installed within the aircraft itself are limited to the system display processor, the power interface to the aircraft, the operator controls, and a global positioning system (GPS) antenna. This design was established to provide a system that could be considered independent of the individual aircraft tail number. It is estimated that all of the internal aircraft mounted units could be installed in less than 2 hours if necessary.

The passive and stabilized hyperspectral sensor collects both spatial (770 pixels) and spectral data (up to 288 pixels) on each instantaneous image increment. The data are binned by 2 spatially and 6 spectrally to give 385 spatial and 48 spectral channels. This imaged data is framed at 50 Hz, with each frame covering a 40-degree lateral field of view and approximately a 0.06-degree (1 milli-radian) field of view in the direction of flight. The data are simultaneously recorded in the archival storage system, processed by the image processor, and presented in a pseudo-color waterfall display to the operator. The processing system evaluates the data sensed in near real time using both spectral and spatial processing, and it provides a "frozen" display of the target along with its position in longitude and latitude. A stabilization system automatically adjusts the sensor so that it compensates for aircraft roll, pitch, and yaw. A "point to track" option forces the stabilization system to point the sensor along a predetermined track (otherwise the sensor points directly down).

These sensors can perform a wide range of ocean sensing tasks. Targets range from submarines and sea mines for military applications, to chlorophyll and sediment load in physical oceanographic applications, to schools of dolphins and whales in marine biology applications. Figure 7 demonstrates the ability of the sensor to image a pod of humpback whales. In these applications and others, a common goal is to detect an extremely low-contrast target in a high-clutter background.

Ocean Environmental Measurements

Hyperspectral systems such as LASH are being developed that use spectral and spatial processing algorithms to discern objects and organisms below the sea surface. The performance of such systems depends on environmental and optical properties of the sea. An instrument suite, the Portable Profiling Oceanographic Instrument System (PorPOIS), was developed to ascertain and quantify these environmental and hydro-optic conditions. Profiling of the downwelling irradiance leads to a value of the diffuse attenuation coefficient, k_d , for the water column. Measurements of the beam absorption, a , and attenuation, c , provide information about the non-pure water absorption and scattering characteristics of the water. Measurement of the backscatter at different wavelengths determines what fraction of the downwelling photons is scattered back toward space. These and a number of other measurements made by PorPOIS allow for a thorough characterization of the water body. These data are used in the LASH program to optimize parameters of the processing algorithms and to predict the performance of the sensor by using modeling software that requires these oceanographic data as inputs.

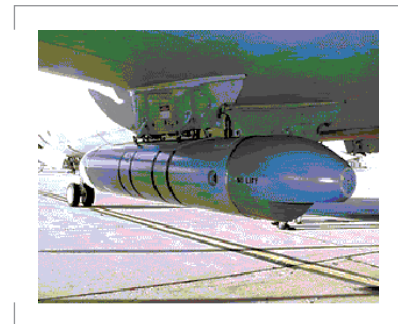


FIGURE 6. LASH pushbroom hyperspectral imager mounted on the wing of a P3 aircraft.

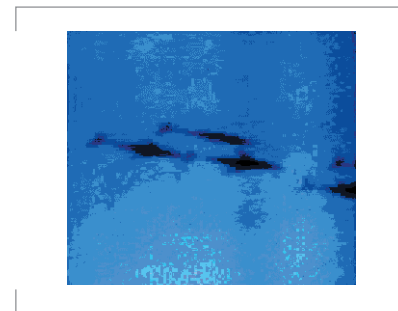


FIGURE 7. A pod of humpback whales imaged using the AAHIS sensor, a precursor to LASH.

The PorPOIS system is deployed on two submersible cages and a surface data-gathering station. The instruments are controlled and the data collected on a laptop computer running a Windows-based control and data acquisition software package, the Sensor Interface Display (SID), developed at SSC San Diego. The instruments (Figure 8) used to measure surface conditions and ship location include a wind transducer (anemometer), a magnetic compass, a surface irradiator, and a GPS receiver. There are currently seven instruments used to measure optical and environmental conditions below the sea surface. These instruments include a downwelling and upwelling irradiator (Biospherical Instruments PER600 and PER700), an upwelling radiometer (PER600), a transmissometer (Seatech), an absorption and attenuation meter (WETLabs ac-9), a conductivity-temperature-depth (CTD) (SeaBird Electronics SBE-19), a fluorometer (WETStar), and a backscattering meter (HobiScat-6). The devices are bundled in a single beehive-type stainless-steel profiling cage as shown in Figure 9. The cage is suspended from a davit via the underwater cable. The SeaBird SBE-32 carousel water sampler (Figure 10) holds twelve 2.5-liter bottles and the SBE-19 CTD. It uses the same underwater cable as the profiling cage. Deployment of the cage is nearly identical to that of the instrument cage. A deck unit mounted in the control rack translates the CTD information from the carousel and transfers the data to SID. This allows the user to capture water samples from target depths by monitoring the position of the carousel as it travels through the water column. New instruments can be added to the configuration as required.

Sample PorPOIS products are shown in Figures 11 and 12. Figure 11 shows downwelling irradiance at 490 nm measured off San Clemente Island, CA. These data are used to determine the rate of attenuation of irradiance at 490 nm, k_{490} , as shown in Figure 12. Optical depth, $1/k_{\lambda}$, is defined as the depth at which surface irradiance of wavelength λ diminishes by $1/e$. System performance is parameterized in terms of optical depth.

SSC San Diego ILIR and ONR-sponsored Research on Hyperspectral Algorithms

Pre-processing transforms are a common initial step in the processing of hyperspectral imagery that is performed in order to determine spectra of the fundamental constituents of the scene or for data compression. The principal component transform is based on minimizing loss in mean-square error, and the vector quantization (VQ) transform is based on minimizing the worst-case angle error between a datum and its projection onto a subspace. These transforms may have unintended consequences on the signal-to-noise ratio (SNR) of a target of interest. We have evaluated the loss in SNR that may result from applying a linear transform and developed several new transforms that use different knowledge of the signals of interest to reduce the loss in SNR in comparison with commonly applied transforms. Figures 13 and 14 illustrate the detectability of an underwater target in data that has been transformed using vector quantization and one of the newly defined transforms, whitened vector quantization (WVQ), that uses no signal information. Clearly, the WVQ algorithm can reduce the dimension of the data and preserve the target SNR for these



FIGURE 8. The Biospherical Instruments PRR-610 surface irradiator, the NEXUS wind transducer, and the NEXUS magnetic compass are used to measure surface conditions.



FIGURE 9. Submersible cage containing instruments used to measure ocean optical properties.



FIGURE 10. Submersible cage containing a CTD and water collection bottles used to measure absorption and scattering as a function of depth.

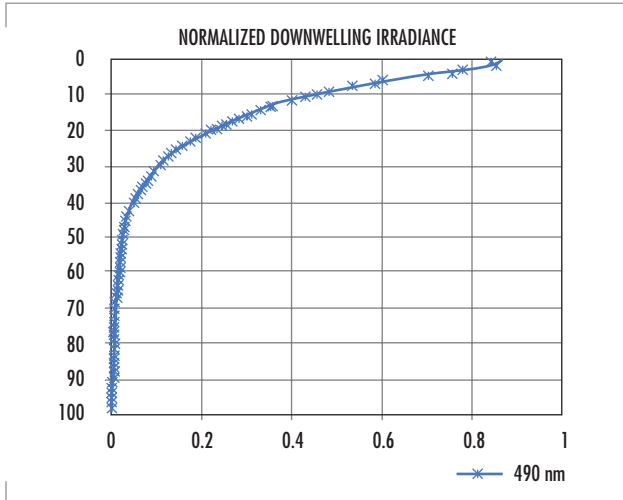


FIGURE 11. Plot of downwelling irradiance at 490 nm as a function of depth as measured using PorPOIS in waters off San Clemente Island, CA.

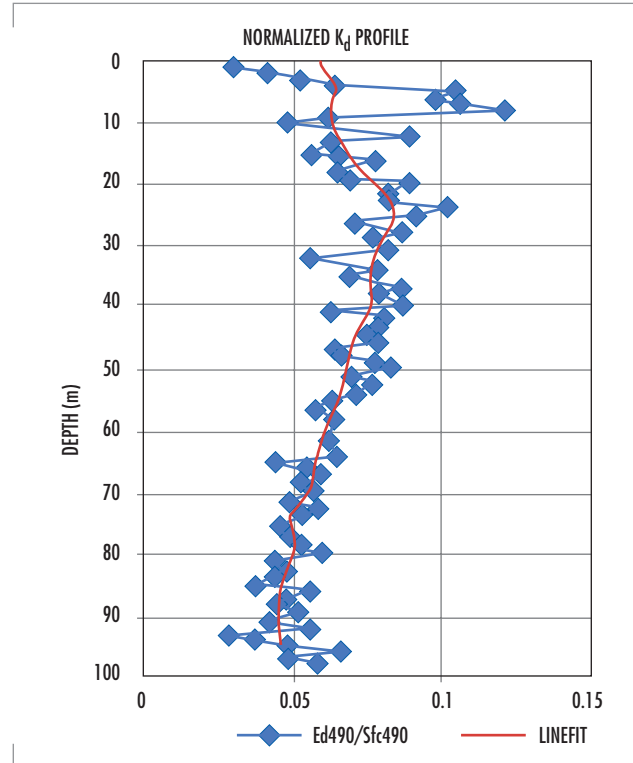


FIGURE 12. Rate of attenuation of downwelling irradiance at 490 nm derived from PorPOIS measurements of downwelling irradiance.

data. The transformed data are processed here with the Reed-Xiaoali (RX) quadratic anomaly detector. The enhanced discrimination of the target at lower dimension using the WVQ algorithm arises from the fact that the performance of quadratic detectors improves for a given SNR if the dimension is reduced.

Linear unmixing and image segmentation are common means of analyzing hyperspectral imagery. Linear unmixing models the observed spectra as

$$y^{ij} = \sum_{k=1}^d a_k^{ij} e_k, \text{ such that } \sum_{k=1}^d a_k^{ij} \leq 1 \text{ and } 0 \leq a_k^{ij} \leq 1.$$

The spectral vectors, e_k are known as endmembers, and a_k^{ij} is the abundance of the k^{th} material at pixel (i,j) . There are several means available for estimating the endmembers. The abundances are usually estimated by solving the constrained least-squares problem.

Image segmentation typically models the observation vector as arising from one of several classes, such that each class has a multi-variate normal distribution. The number of classes, d , is selected and the mean and covariance of the classes $\{(\mu_{\ell k}, \Sigma_k) \mid 1 \leq k \leq d\}$ are estimated from the hyperspectral data. The expectation maximization and the stochastic expectation maximization algorithm are two methods of estimating these parameters. Given the parameters and the probability of each class, the data may be classified by assigning y^{ij} to the class that, conditioned on the observation, is most likely. This computation is carried out using Bayes Law.

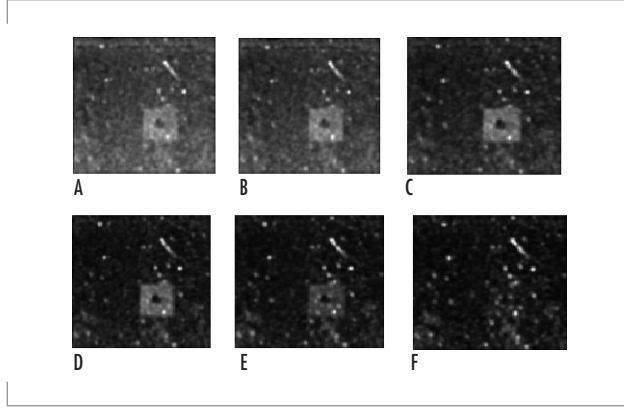


FIGURE 13. The RX algorithm applied to VQ-transformed 48-band hyperspectral imagery transformed to 48, 36, 20, 12, 9, and 7 dimensions (A through F, respectively).

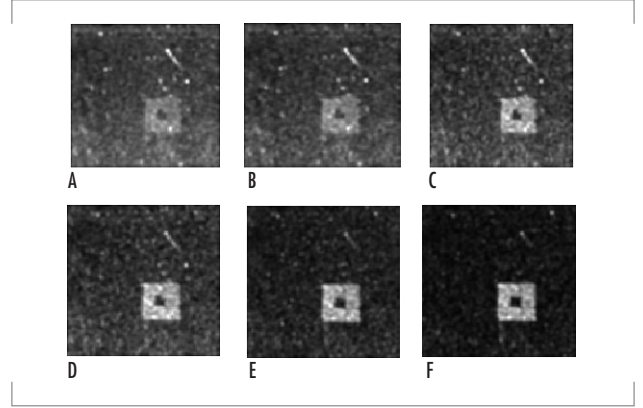


FIGURE 14. The RX algorithm applied to WVQ-transformed 48-band hyperspectral imagery transformed to 48, 36, 24, 8, 4, and 2 dimensions (A through F, respectively).

We have generalized the linear unmixing and image segmentation approaches in the development of the stochastic compositional model. We assume an $A \times B$ image of multivariate data: $y^{ij} \in \mathbb{R}^n$, $1 \leq i \leq A$, $1 \leq j \leq B$. The stochastic compositional approach models each observation vector as a constrained linear combination of normally distributed random variables. Let d be the number of classes, and let $N(\mu_k, \Sigma_k)$, $1 \leq k \leq d$ denote the normal distribution with mean μ_k and covariance Σ_k then

$$y^{ij} = \sum_{k=1}^d a_k^{ij} x_k^{ij} \text{ such that } x_k^{ij} \sim N(\mu_k, \Sigma_k), 0 \leq a_k^{ij} \leq 1, \text{ and } \sum_{k=1}^d a_k^{ij} = 1. \quad (1)$$

To account for scalar variation in the illumination, we also consider the model that uses an inequality constraint:

$$y^{ij} = \sum_{k=1}^d a_k^{ij} x_k^{ij} \text{ such that } x_k^{ij} \sim N(\mu_k, \Sigma_k), 0 \leq a_k^{ij} \leq 1, \text{ and } \sum_{k=1}^d a_k^{ij} \leq 1. \quad (2)$$

For given parameters (μ_k, Σ_k) , $1 \leq k \leq d$, and given abundances

$\alpha = (a_1, \dots, a_d)$, let (dropping the pixel indices) $\mu(\alpha) = \sum_{k=1}^d a_k \mu_k$, and $\Sigma(\alpha) = \sum_{k=1}^d a_k^2 \Sigma_k$. Then, $y^{ij} \sim N(\mu(\alpha), \Sigma(\alpha))$. Maximum likelihood abundance estimates are thus obtained by solving

$$\hat{\alpha}^{ij} = \arg(\max(\frac{1}{|\Sigma(\alpha)|^{0.5} (2\pi)^{n/2}} \exp(\frac{-1}{2}(y^{ij} - \mu(\alpha))\Sigma(\alpha)^{-1}(y^{ij} - \mu(\alpha)))). \quad (3)$$

Let $X = (x_1, \dots, x_d)$; the maximum likelihood estimates of the decomposition of the observation into contributions, x_k from the classes is obtained by solving

$$\begin{aligned} \hat{X} &= \arg(\max(p(X | y, \alpha, \mu_k, \Sigma_k))) \\ &= \arg\left(\max\left(\prod_{k=1}^d \frac{1}{(2\pi)^{n/2} |\Sigma_k|^{1/2}} \exp\left(\frac{-1}{2}(x_k - \mu_k)' \Sigma_k^{-1} (x_k - \mu_k)\right)\right)\right) \\ &\text{such that } y = \sum_{k=1}^d a_k x_k. \end{aligned} \quad (4)$$

The stochastic compositional model and deterministic linear unmixing have been compared by using simulated hyperspectral imagery. Class statistics were estimated from hyperspectral imagery by using the stochastic expectation maximization algorithm. Using these parameters, a set of simulated hyperspectral imagery was generated so that the mixing proportions of the classes were known. The test data were then unmixed by using both deterministic unmixing (with the class means as endmembers) and by stochastic compositional modeling, such that the class parameters were estimated using the expectation maximization algorithm. Figure 15 compares the error in the abundance estimates of one of the classes using the two methods. In this example, the stochastic compositional model reduces the abundance estimation error by a factor of two to three. Work is ongoing to compare the performance of detection algorithms emanating from the segmentation, linear unmixing, and stochastic compositional models.

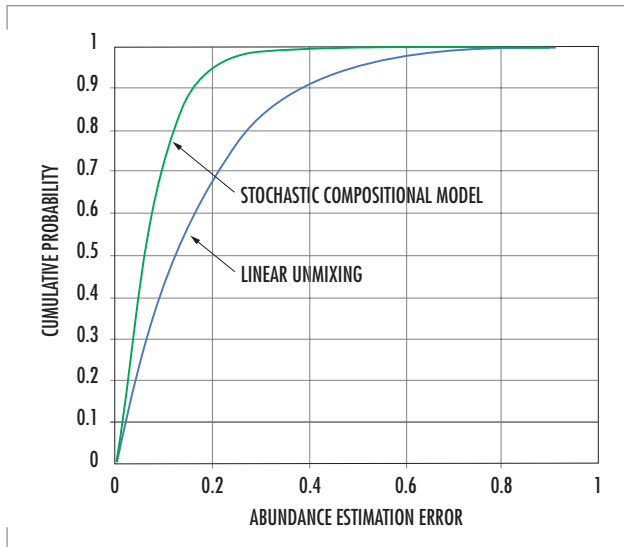
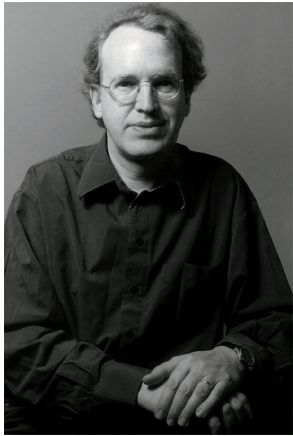


FIGURE 15. A comparison of the absolute error in the abundance estimate using linear unmixing and stochastic compositional modeling.

SUMMARY

SSC San Diego has been involved in many aspects of hyperspectral imaging. We are making important contributions in the areas of real-time processing implementations, system design for a variety of missions, environmental characterization, and the development of new models and methods. SSC San Diego is continuing to work across the Department of Defense (DoD)/Intelligence communities to bring mature hyperspectral technologies to the warfighter, making this unique source of critical information more widely available and user friendly.

**David Stein**

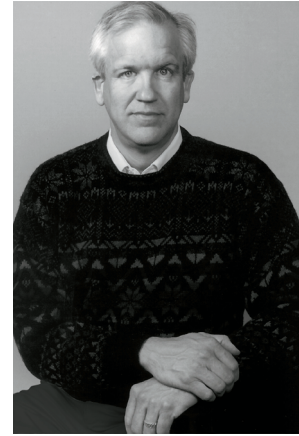
Ph.D. in Mathematics, Brandeis University, 1986

Current Research: Multidimensional statistics; detection theory; hyperspectral algorithms; remote sensing of littoral processes.

**Jon Schoonmaker**

BS in Physics/Mathematics, University of Oregon, 1985

Current Research: Hyperspectral systems; data analysis and algorithm development; remote sensing of littoral processes.

**Eric Coolbaugh**

MS in Oceanography and Meteorology, Naval Postgraduate School, 1989

Current Research: Hyperspectral imaging systems; high-performance computing; hyperspectral algorithms.